Proceedings of the
Annual Stability Conference
Structural Stability Research Council
Atlanta, Georgia, April 21-24, 2020

New formulations for the cross-sectional strength of high-strength steel rectangular and square hollow sections using a generalized slenderness-based resistance method

Andrea Toffolon[1], Andreas Taras[2]

Abstract
Light-weight spatial structures with high demands for aesthetics, structural strength and stability may very efficiently be built using high-strength steel Rectangular Hollow Sections (RHS) or Square Hollow Sections (SHS). Currently, the use of these sections is partly hindered by an underlying over-conservatism in design rules for local buckling of the cross-section, since most high-strength steel sections are slender with regards to local buckling. This paper illustrates a novel approach for the design of thin- to thick-walled RHS and SHS against elastic and elasto-plastic local buckling. It introduces a "Generalized Slenderness-based Resistance Method" (GSRM), which was developed over the course of an extensive, multinational and EU-funded research project – HOLLOSSTAB (2016-2019). The method further generalizes advanced cross-sectional definitions of local and global slenderness, ultimately providing a strength-based resistance approach that generalizes the concepts of established design methods such as the Direct Strength Method. In the GSRM, the slenderness and buckling resistance are both based on the section elastic resistance and incorporate the overall applied load case. This new format is used as the basis for the derivation of new design rules, which were developed through an extensive parametric study and mechanical model calibration. The presented study also includes an analysis of the underlying level of the reliability of the GSRM design rules and compares its advantages over conventional design methods for square and rectangular sections especially for slender cross-sections loaded by general direct stresses caused by compression and arbitrary bi-axial bending.

1 Introduction

1.1 General remarks and scope

In recent years, it was regularly observed that current design standards lack in accuracy and economy when applied to High-Strength Steels and more complex load cases, even for – at first sight – well understood section types such as hollow structural sections (HSS). This has been observed by several authors for the European codes (*Eurocode3 2006*), where a lack of accuracy and – sometimes – also safety of design rules based on the Winter curve (*Winter 1946*) and applied to the design of box and rectangular hollow sections was noted (see e.g. *Schillo et al. 2018*). Similar

[1] Graduate Research Assistant, Bundeswehr University Munich, <andrea.toffolon@unibw.de>
[2] Professor – Steel and Composite Structures, ETH Zurich, Institute of Structural Engineering, <ataras@ethz.ch>

observations also apply to North American standards (e.g. *ANSI/AISC 2016* and *AISI 2016*). In all these standards, albeit due to different reasons, the inaccuracies are most pronounced in the presence of combined loading (compression and uni- or bi-axial bending). This paper describes a new methodology for the cross-sectional design checks of SHS and RHS, the *Generalized Slenderness-based Resistance Method* (GSRM). This method was developed over the course of the EU-funded (RFCS) research project HOLLOSSTAB (*Taras et al. 2019*), as part of a wider effort to better understand the behavior and strength of hollow sections and improve the economy and practicality of design rules dedicated to these types of section. The method thereby reprises concepts found in methods such as the ones used in Eurocode 3's "General Method", the Overall Interaction Concept - OIC (*Boissonnade et al. 2017; Kettler et al. 2009*), the Direct Strength Method – DSM (*Schafer 2008; Schafer 2018*) and the Continuous Strength Method - CSM (*Gardner, 2008;* see also *Afsahn and Gardner 2013*; *Yun and Gardner 2018a; Fieber et al. 2019*). The commonality of these methods is that they make use of a more generalized definition of slenderness, which is usually determined with the aid of dedicated numerical tools, as the main input parameter for the calculation of strength, which in turn is given as a (direct) function of this slenderness. The GSRM developed during HOLLOSSTAB is a dedicated, new design rule, based on slenderness definitions of this type, which may be applied to various types and shapes of hollow sections and for cross-sections as well as members.

The present paper is structured in a manner that closely follows the various steps taken in HOLLOSSTAB for the development and validation of the new GSRM design rules for cross-sectional design checks. The first part of the paper briefly describes the physical test campaign and the numerical parametric study of the cross-sectional strength of SHS and RHS carried out within the project. This work formed the basis for the subsequent formulation, calibration and validation of the new GSRM design rules, which are described in the second part of the paper. Finally, quantitative comparisons between the levels of accuracy of current Eurocode 3 (EC3), AISC design rules and the GSRM are given. The present paper specifically focuses on the development of GSRM design rules for the cross-sectional strength of square or rectangular HSS. The reader may also refer to *Meng et al.,* (*2019*) for an analogous treatment of the cross-sectional capacity of circular and elliptical hollow sections.

1.2 Basic concepts of the GSRM

The GSRM, in its application to cross-sectional design checks, is a method that makes use of an overall definition of the local buckling slenderness, valid for the cross-section as a whole and derived from elastic (numerical) bifurcation analysis. On its basis, it provides a continuous representation of strength throughout slenderness ranges. A schematic graphical representation of the method as applied to cross-sectional resistances (local buckling, index "L") is given in Fig. 1. In addition to the variables described in detail below, the figure makes use of the following parameters:

N	applied axial compressive force
N_{pl}	plastic compressive capacity of the gross cross-section $N_{pl}=Af_y$
f_y	yield stress
M	applied bending moment
M_{el}	elastic bending moment resistance, $M_{el} = W_{el} f_y$
M_{pl}	plastic bending moment capacity, $M_{pl} = W_{pl} f_y$

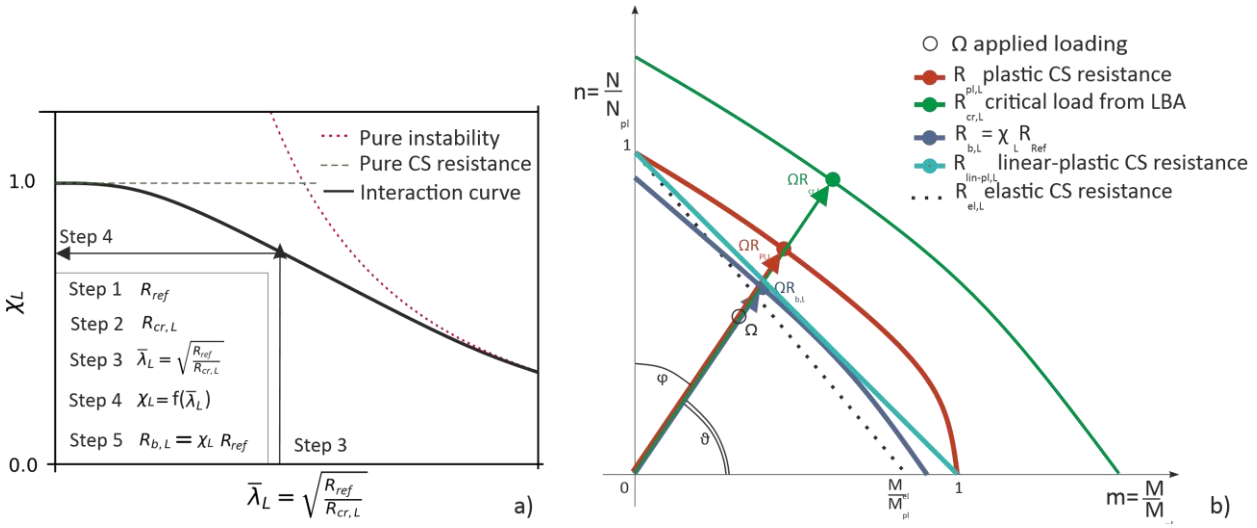

Fig. 1: Graphical representation of the GSRM design approach for cross-sectional resistance / local buckling "L": (a) strength curves in the χ_L - $\bar{\lambda}_L$ plane and (b) n-m interaction curves.

The following steps and procedures are involved in the GSRM-based strength design of cross-sections:

1. Calculation of a cross-sectional reference resistance, R_{ref}, associated with the stress field stemming from the load case under consideration, which is a combination of axial force and bending defined by a vector length Ω and an angle φ in the n-m plane, respectively two angles φ_y and φ_z in the n-m_y-m_z space. Owing to the greater ease of representation, the in-plane case is illustrated, see Fig. 1b). While in principle these quantities could be defined in a variety of different ways, in this plot n and m are the axial force and bending moment normalised with respect to the corresponding ideal plastic resistances (yielding in all fibres).

$$\varphi_y = \arctan\left(\frac{m_y}{n}\right) \quad \varphi_z = \arctan\left(\frac{m_z}{n}\right) \tag{1}$$

Where

$$m_y = \frac{M_{y,Ed}}{M_{y,pl}} \quad ; \quad m_z = \frac{M_{z,Ed}}{M_{z,pl}} \quad ; \quad n = \frac{N_{Ed}}{N_{pl}} \tag{2}$$

The reference resistance R_{ref} must be defined in a uniform manner in the GSRM. Both the plastic resistance R_{pl} and the elastic resistance R_{el} fulfil this basic requirement. Thereby, R_{pl} is the load amplification factors for the considered load case needed to reach the theoretical ideal-plastic condition (yielding in all fibres, no strain hardening), while R_{el} defines the first yield load (yielding in one extreme fibre of the cross-section). As will be discussed in more detail in the paper, for the GSRM the elastic quantity R_{el} was finally chosen as the reference resistance.

2. Calculation of the cross-section (local) critical elastic bifurcation/buckling load factor, $R_{cr,L}$, which once again is associated with the same stress resultant profile defined in the previous item.
3. On the basis of the two values calculated in the two previous items, calculation of the cross-sectional (local) slenderness, defined as:

$$\bar{\lambda}_{\mathrm{L}} = \sqrt{\frac{\mathrm{R_{ref}}}{\mathrm{R_{cr,L}}}} \tag{3}$$

4. Retrieval of the buckling factor χ_L from a pre-determined set of equations. The functions and equations that determine the values of the buckling factors χ_L (for local buckling) or χ_G (for global, member buckling) are the key component of a design method such as the GSRM. In HOLLOSSTAB, they were developed for the cross-sectional as well as the member buckling strength of hollow sections of various shape and steel grade.
5. Determination of the buckling strength $R_{b,L}$ by the following formula:

$$R_{\mathrm{b,L}} = \chi_{\mathrm{L}} R_{\mathrm{ref}} \tag{4}$$

Concerning the above steps and procedures, the following additional comments should be considered:

i. R_{ref} and $R_{cr,L}$ may be calculated by means of available analytical expressions, for very simple load cases, or through numerical analysis, for more general load cases. In the latter case, it is fruitful to develop dedicated software tools, as was done in HOLLOSSTAB.

ii. On the other hand, the value of $R_{cr,L}$ may be obtained for a simply supported member of length corresponding to the first buckling wave length $L_{cr,L,n=1}$ and a uniform stress distribution along this length; it is thus not necessary to consider the particular end support conditions and stress distribution along the considered member.

iii. In addition to the mentioned resistance factors, other parameters related to the cross-section properties are needed to define the strength curves in both the slender and the stocky ranges. For example, in the stocky range, the plastic resistance of the cross-section R_{pl} is also a parameter of interest, even though it is not directly used in the slenderness definition of the GSRM.

2 Experimental campaign

Among the various hollow section types considered by the research partners in HOLLOSSTAB, cold-formed and hot-finished SHS and RHS, as shown in Fig. 2, made of mild or high-strength steel, were tested at the laboratories of structural engineering of Bundeswehr University Munich (BWU), Imperial College London (ICL) and Técnico Lisboa (IST). A total of 97 tests on short columns and beam-columns were conducted between the three laboratories in order to provide the full-scale experimental evidence for the development of numerical models and GSRM design rules for the cross-sectional resistance of such components. The test methodology and main results obtained in the subset of the test campaign of HOLLOSSTAB that was carried out at BWU will be briefly discussed in the following, thereby exemplifying the procedure generally adopted at all involved laboratories in the project. Full details on the experimental campaign on SHS, RHS and derived hollow section shapes can be found in the published documentation of the HOLLOSSTAB project (*Taras et al., 2019*).

Cold-formed SHS and RHS (in addition to several derived sections such as hexagonal sections and groove-stiffened SHS, see also *Toffolon et al. 2019a*) were studied at the structural laboratory of BWU. The sections' outer dimensions and wall thicknesses were chosen by keeping in mind the general objective of the HOLLOSSTAB project, which was to provide design rules that lead to improvements particularly for more slender sections, i.e. mainly class 3 and 4 sections according

to Eurocode 3. Of the six RHS /SHS tested at BWU, four were made of S355 steel, while two were cold-formed higher strength steel sections with measured values of the yield stress of above $R_{p0,2}$=700 N/mm².

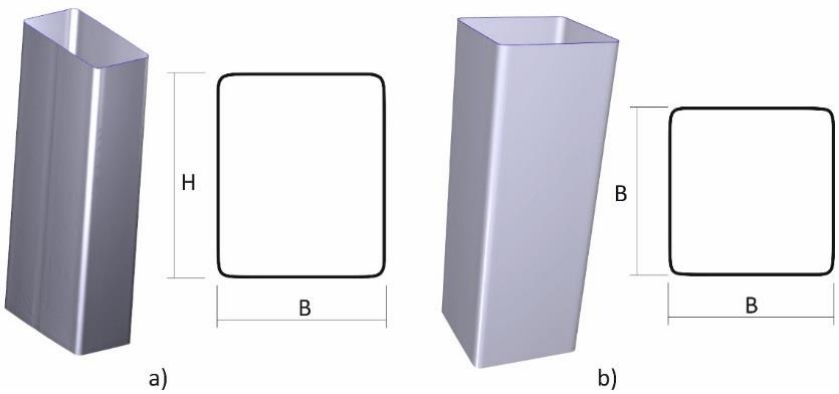

Fig. 2: Scope of this paper: cross-sectional strength of square and rectangular hollow sections (SHS, RHS) fabricated acc. to EN 10219 (cold-formed sections) or EN10210 (hot-finished sections) with steel grades from (normal strength) S355 to (high strength) S770.

The full-scale experimental tests on local buckling at BWU comprised two test setups: stub-column tests and short beam-column tests. Different levels of eccentricity were applied to obtain different combinations of axial compression and bending moment. The full-scale tests were performed in a 10 MN servo-hydraulic test rig, where the load cells incorporate a linear variable displacement transducer and a pressure transducer, see Fig. 3a. A digital image correlation system (DIC) produced by GOM was used to monitor deformations and rotations of the specimen surfaces and of the test rig itself. These measurements were also compared to test data from inclinometers and strain gauges applied to the specimen.

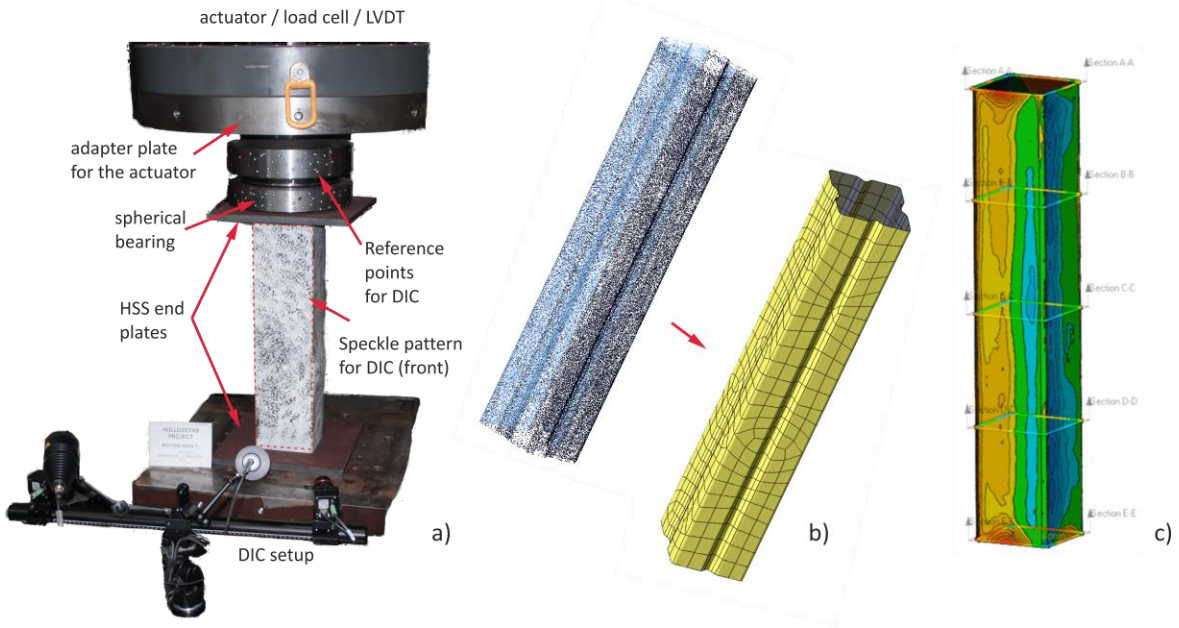

Fig. 3: a) test setup for the stub-column test, b) point cloud of the 3D scan data, c) 3D results of measuring system of a SHS specimen.

For each specimen, the experimental campaign also included auxiliary tests such as tensile coupon tests and imperfection measurements. These were carried out in order to have sufficient information on each test to perform an accurate validation of numerical models, see the following section, which in turn were used for an extensive parametric study. Additionally, a 3D scanning technique was employed to measure the distribution of local geometric imperfections in each test specimen. The real geometry of the specimen including imperfections was then used in the numerical simulation by laying spline surfaces on the cloud points from the 3D scanning measurement, as is shown in Fig. 3b. Additionally, the 3D scan data were statistically evaluated with respect to shape deviations and tolerances from the nominal geometry. Fig. 3c demonstrates an example of the evaluation of a SHS specimen.

3 Validation and calibration of the numerical model

3.1 General remarks

The principal aim of the experimental campaign was to provide the basis for the validation of advanced numerical models that use Geometrically and Materially Non-Linear FEM-Analyses with Imperfections (GMNIA) to realistically and accurately simulate the behaviour of the studied sections loaded in compression and bending. The development and validation of these Finite Element Method (FEM) models was thus performed through comparisons with the experimental tests. This reverse engineering process, using GMNIA analyses with the measured geometrical shape of the sections and an accurate material model, can lead to very small (<3%) deviations to the ultimate load of the buckling tests if the meshing and modelling of boundary conditions are accurate. This type of GMNIA, which uses measured input data and was performed during the reverse engineering and model validation phase, is denoted by "GMNIA-MEAS" in the following. The proprietary software Dassault Simulia *ABAQUS* (*2016*) was used for all numerical simulations, employing linear isoparametric shell elements with reduced integration (element type S4R). As a result of the model validation, a mesh density with a minimum of 60 elements in circumferential and 200 elements in longitudinal direction was found to lead to converging results of high accuracy.

An example of an FEM model validation is shown in Fig. 4. The RHS specimen deformed shape in a) was caused by an eccentric compressive load and the deformations were measured by a GOM (Aramis) DIC system. The corresponding GMNIA-MEAS is able to reproduce both the position and shape of the post-buckling deformations as well as the peak load itself quite accurately, see Fig. 4b) and c). As the figure also illustrates, the load-shortening and load-rotation paths obtained from the FE models were typically too stiff up to the peak load and descended more rapidly than in the experimental observation. For the purposes of the project, these deviations in the load-deformation paths were not of concern, as the peak value of resistance was the main value against which the models were validated. Full details on the model validation and calibration may be found in *Taras et al.* (2019), *Toffolon et al.* (2019b).

In summary, the following statistics of the model validation were obtained:

- for the 12 stub-column tests (pure axial compression) conducted at BWU and considered here, the average of the ratio between the peak load in the validated GMNIA-MEAS models and the experimental tests was $F_{max,FEM}/F_{max,test}=0.99$, with a standard deviation of

3.2%.

- for the total of 48 BWU stub-column and short beam-column tests on RHS/SHS and derived section shapes, an average value of $F_{max,FEM}/F_{max,test}$=0.99 was obtained, with 4.2% standard deviation.

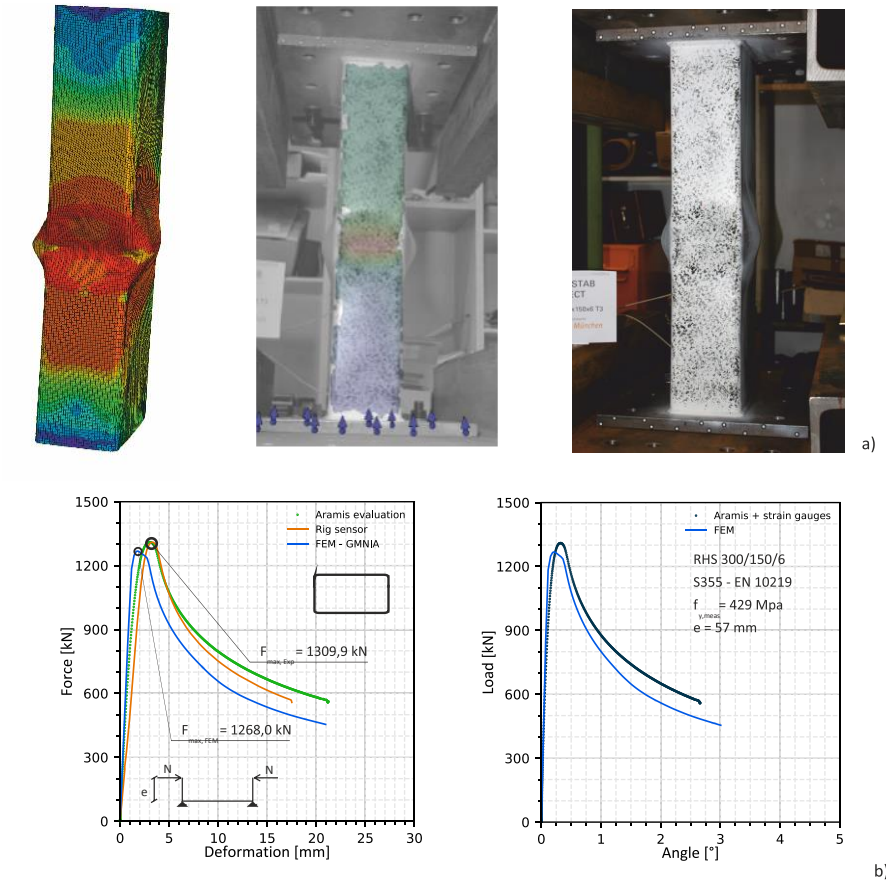

Fig. 4: a) GMNIA-MEAS model vs. test results, specimen deformed shape measured with DIC; b) Load-deformation and load-rotation plots.

While the experimental campaign carried out in HOLLOSSTAB was extensive, it nevertheless could not cover the full range of section shapes, material grades and – most importantly – combinations of compression forces and bi-axial bending moments that the new GSRM design rules need to cover. For this reason, an exhaustive numerical parametric study was carried out, thus providing the otherwise missing comprehensive database of test results via numerical tests. The scope and employed methodology of the parametric study is described in this section, while the results are mainly illustrated in the context of the development of the GSRM design rules, where they provide the basis for comparisons with the new design proposals.

3.2 Methodology – simplified model with equivalent imperfections

In order to make the parametric study efficient, the previously described GMNIA-MEAS models had to be simplified with regards to the modelling of imperfections and material laws. Thus, a more generalized model, with a simplified definition of the material law and the geometrical imperfections, yet the same FEM mesh size and element types as the ones validated through the calibration to the experimental tests, was developed. In a first step, the geometrical input was

calibrated. Thereby, the GMNIA-MEAS load-deformation curves described in the previous section were compared to different GMNIA calculations with nominal cross-sectional geometry (outer dimensions) and varying *equivalent* imperfection amplitudes. The first buckling mode of a Linear Buckling Analysis (LBA) represents a sensible and well-established basis (see e.g. Annex C of *Eurocode 3 Part 1-5 2006*) and is chosen as input for the imperfection calibration for the GMNIA.

A representative example for this calibration is shown in Fig. 5, where the load-deformation curves for two different SHS sections are shown and the GMNIA-MEAS curves are compared to GMNIA curves obtained from an analysis with an equivalent geometric imperfection based on a scaled (by the indicated value of e_0) first buckling mode for local buckling, obtained from an LBA. The same material model (taken from tensile tests) was used for both calculations, thus allowing for an isolation of the effect of imperfections on the obtained peak loads. The imperfection amplitudes in this figure range from B/400 up to B/150, where B is the external width of the SHS. The figure illustrates the moderate sensitivity of the peak load to variations of the LBA buckling mode scaling factor e_0.

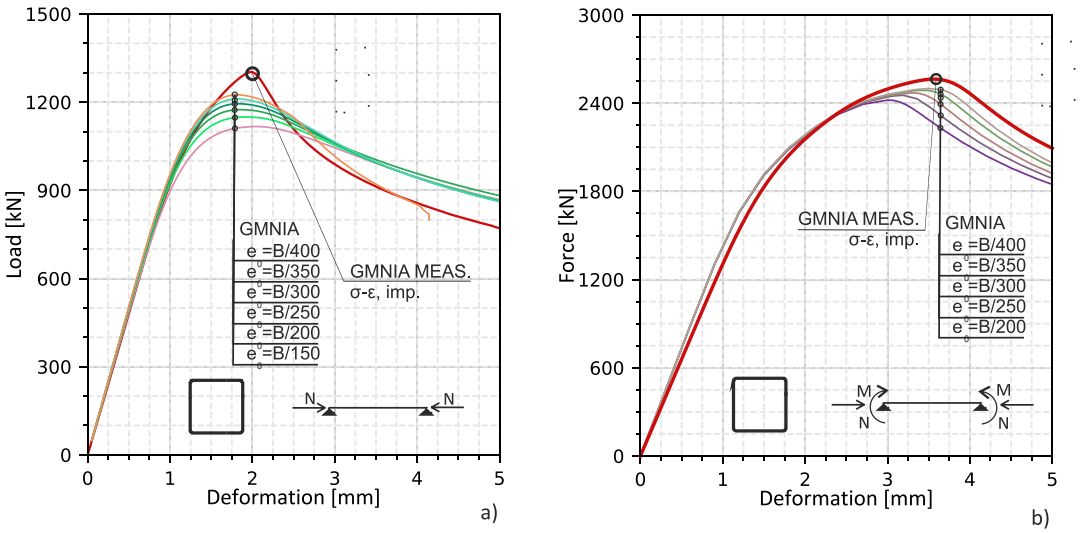

Fig. 5: calibration of the imperfection amplitude for a a) SHS 200×200×5 S355 (pure compression), and b) SHS 200×200×8 S355 (compression + bending)

Finally, a value of e_0=B/400 was chosen, as this value was taken to be generally more representative for the local buckling behaviour of these SHS, RHS, SHS-S and SHS-T sections than the value of e_0=B/200 recommended for design tasks in Eurocode design provisions (Annex C of *Eurocode 3 Part 1-5, 2006*). This is also in line with the findings of e.g. *Rusch and Lindner* (2001): they determined that amplitudes of B/400 are most suitable to represent the so-called Winter curves (*Winter, 1946*) for local buckling in numerical analyses. An assessment of the reliability level of the design rules in the Eurocodes was recently carried out in *Schillo et al. 2018*, highlighting inhomogeneity caused by the discontinuities in current design rules for hollow and box sections of various shapes.

An overview and summary of the aforementioned model assumptions and chosen procedure for the FEM parametric study is given in Fig. 6. Thereby, Fig. 6b) and c) schematically represent the first buckling mode for an exemplary SHS and RHS subjected to different load combinations. In

part a) of the figure, a material model specifically developed by *Yun and Gardner* (2017, 2018) for the stress-strain relationship of hot-finished and cold-formed sections are shown. These were finally used in the parametric study, using the nominal values of the yield stress and tensile strength for each considered material. The use of these material models also has the added advantage that it manages to reproduce the effects of residual stresses on the buckling strength in an overall manner. For a more detailed description of this aspect and of the calibration of the GMNIA model the reader may refer to *Taras et al.* (2019a).

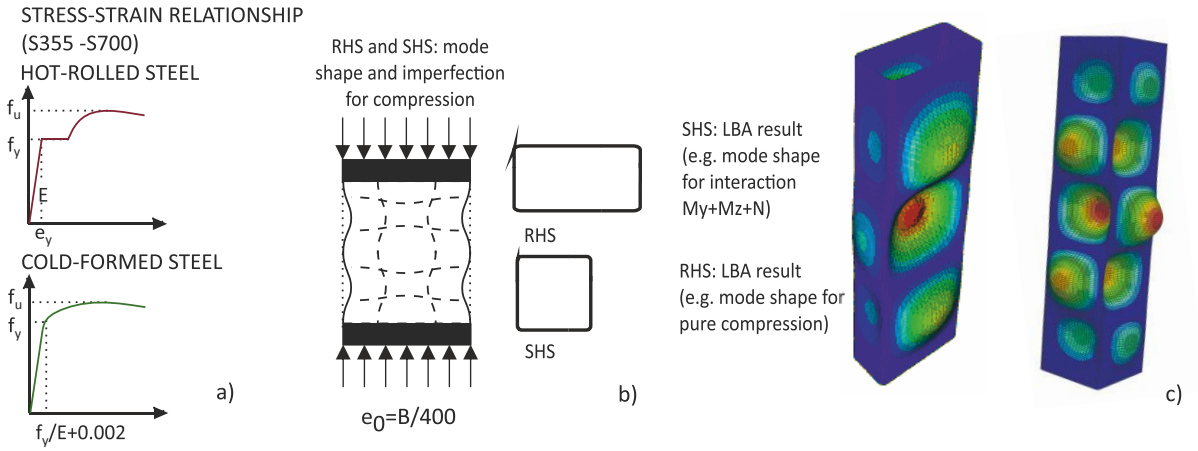

Fig. 6: Material model chosen for the EN10219 and EN10210 standards; b) cross-section shapes; c) LBA shape for the local imperfections

4 Parametric study – overview of input parameters and results

The aim of the numerical parametric study on the local buckling behaviour of slender and non-slender cross-sections was the realistic determination of the cross-section capacity under different load combinations and for various degrees of local slenderness. For this reason, a large number of thicknesses and load combinations was considered. The numerical test campaign conducted for the study of local buckling of SHS and RHS alone therefore consisted of around 30000 numerical tests (LBA+GMNIA), the parameters of which are shown in Table 1 in form of a test matrix. All shown parameters were combined with each other in the numerical test programme.

Table 1: Parameters of the parametric study on local buckling

Thickness (mm)	L/L_{cr} (-)	Steel grade	Local Imperfection amplitude	ϕ_y (°)	ϕ_z (°)	H/B (-)	Manufacturing standard
2.0	0.1	S355	B/400	0	0	1	EN10219
2.5	0.15	S460		15	15	1.5	EN10210
3.0	0.2	S550		30	30	2	
3.5		S700		45	45		
4.0				60	60		
5.0				75	75		
6.3				90	90		
8.0							
10.0							
12.0							

Thereby, in the table, the following variables are used:

$$\frac{L}{L_{cr}} = min\left(\frac{I_y}{A};\frac{I_z}{A}\right)\pi\sqrt{\frac{E}{f_y}} \quad ; \quad \phi_y = arctan\left(\frac{m_y}{n}\right) \quad ; \quad \phi_z = arctan\left(\frac{m_z}{n}\right)$$

An overview of the results of the extensive parametric study for the local buckling of SHS and RHS is given in Fig. 7. For a graphical representation of the results, the $\bar{\lambda}_L$ / χ_L plot was chosen. This representation shows the obtained ultimate strength through the factor χ_L, which is the ratio between the ultimate strength $R_{b,L}$ at the cross-sectional level divided by a reference resistance $R_{ref,}$ plotted over a generalized slenderness for the cross-sectional (local buckling) strength $\bar{\lambda}_L$. Each point in Fig. 7 represents a single result obtained from a GMNIA as described above. The results are marked with colours other than red for special load cases, such as pure compression, pure bending about the y and z-axis. Two definitions of the reference resistance R_{ref} and thus of $\bar{\lambda}_L$ and χ_L are chosen for the data representation in this figure:

in Fig. 7a

$$\bar{\lambda}_L = \sqrt{\frac{R_{pl}}{R_{cr,L}}} \tag{5}$$

and

$$\chi_L = \frac{R_{GMNIA}}{R_{pl}} \tag{6}$$

in Fig. 7b

$$\bar{\lambda}_L = \sqrt{\frac{R_{el}}{R_{cr,L}}} \tag{7}$$

and

$$\chi_L = \frac{R_{GMNIA}}{R_{el}} \tag{8}$$

The plots clearly illustrate that quite different values of χ_L are obtained depending on the definition of R_{ref}. Fig. 7a) at first glance seems to indicate a relatively compact scatter band in the R_{pl} - based representation. However, the differences between various χ_L values at a particular slenderness are still pronounced, and a simple lower-bound curve would underpredict many capacities by up to 50%. The most common load cases, such as pure compression or bending moments, are positioned in the higher range of the scatter band for this type of representation, with the pure compression case showing a similar pattern to the pure bending case. This implies that safe-sided design rules based on R_{pl} would mostly be governed by less common cases with high load eccentricities. Different results are obtained if the cross-section reference resistance is given by R_{el}, with the corresponding changes in the definitions of slenderness and knock-down factor. At first, the scatter in the corresponding Fig. 7b) appears wider, since very high values of χ_L are reached, mainly due to the high difference between R_{el} and R_{pl} in bi-axially bent sections. However, as was observed during the development of GSRM design rules in HOLLOSSTAB, much clearer patterns emerge if R_{el} is chosen as reference resistance. Very advantageously for the development of practical design curves, a description with "Winter-type formulae" is made possible, since most of the results follow the pattern of the plotted Winter curve. Conveniently, the standard cases of pure compression and pure bending are near the lower bound of resistances. For this reason among others, R_{ref}=R_{el} was finally chosen in HOLLOSSTAB for the representation of the results of the numerical parametric study and of the design rules developed from it.

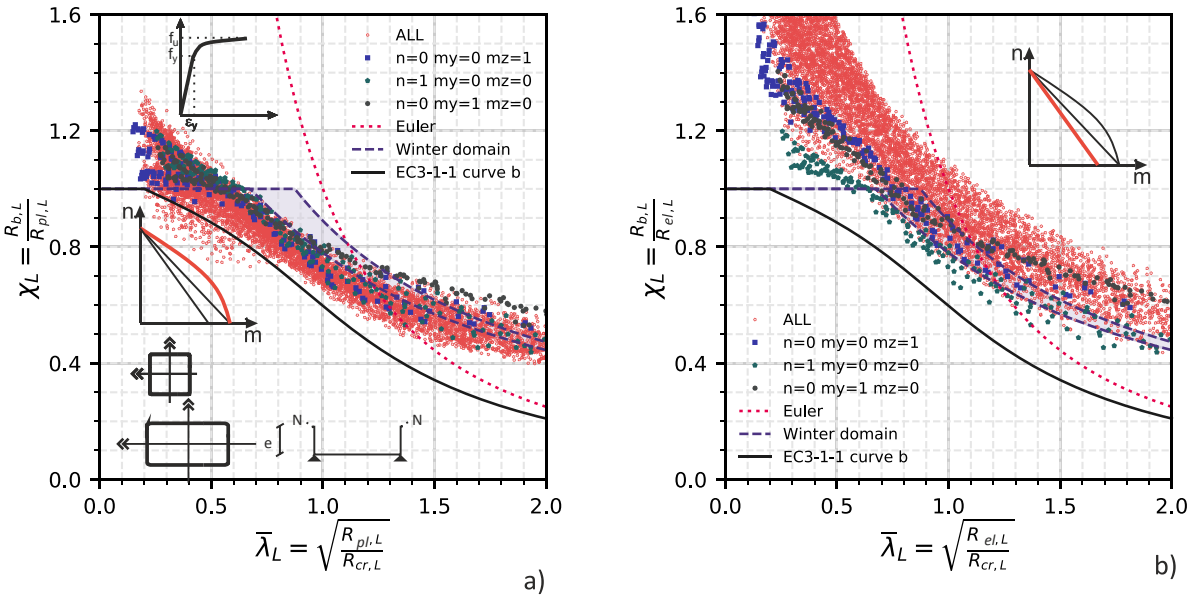

Fig. 7: Overview of all results of the parametric study on the cross-sectional (local buckling) strength for cold-formed RHS & SHS; a) representation of the GSRM buckling knockdown factor using R_{pl} as reference resistance; b) representation using R_{el}.

5 Development and calibration of GSRM design formulae

The spread of plasticity that sets on after the exceedance of the yield stress in the outermost fibre is a dominant factor in any stability problem in the elastic-plastic transitional range. For this reason, even though the GSRM eliminates the concept of cross-sectional classes as currently found in most design codes, it is still necessary to distinguish between sections that may reach and exceed the elastic resistance R_{el} and those that will reach the peak load before this point is reached. (Incidentally, this is an additional advantage of the choice of R_{el} as the reference resistance R_{ref} in the GSRM). The development and calibration of new, GSRM-type design formulae was thus carried out for two distinct ranges. In the following sub-section 5.1, the GSRM design curve for the elastic range will be derived from the theory of plate buckling and the calibration of modified Winter formulae, familiar from plate buckling cases as defined in most international standards (e.g *Eurocode 3 Part 1-5, 2006*). For the "plastic" range of slenderness, a different formulation is provided in 5.2 as a simplified and calibrated linear function.

5.1 Winter-type rules in the elastic range

Early studies on plate buckling investigated the simplified model of a thin plate (high width to thickness ratio) supported on both sides and subjected to a constant in-plane compression load. The reduction factor ρ and the plate slenderness $\bar{\lambda}_p$ can thus be defined as follows:

$$\rho = \frac{B_{eff}}{B} \tag{9}$$

$$\bar{\lambda}_p = \sqrt{\frac{f_y}{\sigma_{crit}}} \tag{10}$$

This formula makes use of the following parameters:

B_{eff}	effective width according to the *Eurocode 3 Part 1-5* (2006) definition.
σ_{crit}	critical stress according to the *Eurocode 3 Part 1-5* (2006) definition.

Using the terms $\bar{\lambda}_p$ and ρ, the plate buckling knock-down factor according to Winter reads:

$$\rho = \frac{1}{\bar{\lambda}_p}\left(1 - \frac{0.22}{\bar{\lambda}_p}\right) \tag{11}$$

where the coefficient 0.22 was finally chosen after different calibrations and proposals (*Winter 1946*). The Eurocode method for plate buckling applies the findings of Winter and assesses separately ρ for each plate of the cross-section (each considered to have simplified, hinged boundary conditions), introducing the parameter ψ, as the ratio between the stress along each plate. The reduction factor and the plate slenderness are defined as follows in *Eurocode 3 Part 1-5* (2006):

$$\rho = \frac{1}{\bar{\lambda}_p}\left(1 - 0.055\frac{3+\psi}{\bar{\lambda}_p}\right) \tag{12}$$

$$\bar{\lambda}_p = \sqrt{\frac{f_y}{\sigma_{crit}}} = \frac{\bar{b}/t}{28.4\sqrt{\frac{235}{f_y}}\sqrt{k_\sigma}} \tag{13}$$

The chosen approach for the GSRM design rules developed in HOLLOSSTAB makes use of the basic structure of Winter's formulae, generalising it to describe the behaviour of the entire cross-section as observed in the project's physical and numerical tests. The slenderness and the reduction factors refer to the cross-section properties (geometry and steel grade) and to the applied load. Thus, in order to use the Winter formulation and fit it to the results of the parametric study, ρ and $\bar{\lambda}_p$ are rewritten as χ_L and $\bar{\lambda}_L$ in the GSRM:

$$\chi_L = \frac{1}{\bar{\lambda}_L}\left(1 - \frac{A}{\bar{\lambda}_L}\right) \tag{14}$$

Thereby, the parameter A was calibrated to the results of the extensive numerical parametric study on local buckling. In this calibration, it was seen to be conducive to good results to define A as a function of ψ_1 and ψ_2, in partial reference to the Eurocode approach. ψ_1 and ψ_2 are the stress ratios in the two plates adjacent to the corner with the highest compressive stress in the section (see Fig. 8) and are defined as follows:

$$\Psi_1 = MAX\left(\frac{\frac{N}{A}+\frac{M_y}{W_{el,y}}-\frac{M_z}{W_{el,z}}}{\frac{N}{A}+\frac{M_y}{W_{el,y}}+\frac{M_z}{W_{el,z}}} \;;\; \frac{\frac{N}{A}-\frac{M_y}{W_{el,y}}+\frac{M_z}{W_{el,z}}}{\frac{N}{A}+\frac{M_y}{W_{el,y}}+\frac{M_z}{W_{el,z}}}\right) \tag{15}$$

$$\Psi_2 = MIN\left(\frac{\frac{N}{A}+\frac{M_y}{W_{el,y}}-\frac{M_z}{W_{el,z}}}{\frac{N}{A}+\frac{M_y}{W_{el,y}}+\frac{M_z}{W_{el,z}}} \;;\; \frac{\frac{N}{A}-\frac{M_y}{W_{el,y}}+\frac{M_z}{W_{el,z}}}{\frac{N}{A}+\frac{M_y}{W_{el,y}}+\frac{M_z}{W_{el,z}}}\right) \tag{16}$$

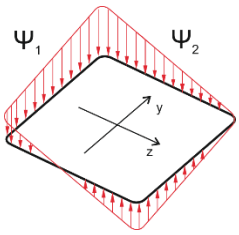

Fig. 8: Definition and graphic representation of ψ_1 and ψ_2 as used in the GSRM formulation for the cross-sectional capacity of SHS and RHS

ψ_1 and ψ_2 may be determined in a simplified manner, discounting the presence of the typical rounding at the edges of SHS and RHS sections, or more precisely, without significantly changing the accuracy of the method. This is justified by the small difference in the actual stress state and the increased use of ease of the formulations. In an initial step, a formulation for the parameter A was sought that describes the cases with compression and mono-axial (or "in-plane") bending, about either axis. This corresponds to all cases where the stress ratio ψ_1 is equal to 1,0 (pure compression in one of the plates). For cold-formed (*EN 10219*) and hot-finished sections (*EN 10210*), the following linear functions were determined through calibration and the final choice of practical, easy-to-use functions and coefficients.

$$A = 0.225 + 0.025\,\psi_2 \text{ (cold-formed sections)} \quad (17)$$

$$A = 0.20 + 0.02\,\psi_2 \text{ (hot-finished sections)} \quad (18)$$

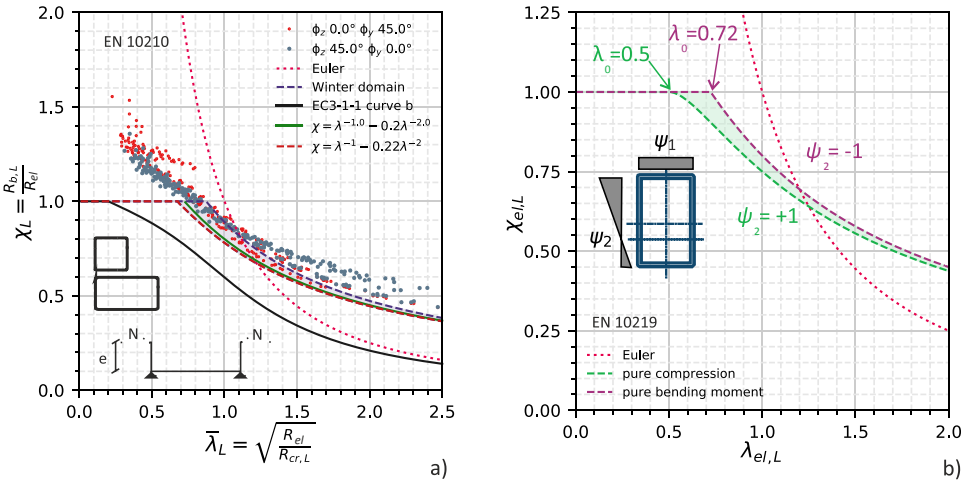

Fig. 9: a) exemplary calibration (mono-axial case) for hot-finished sections; b) overview of the GSRM design curve (mono-axial case) for cold-formed sections.

The validation of these calibrated functions for an exemplary combined N+M_y load case for hot-finished sections is shown in Fig. 9a). In Fig. 9b), the resulting range of possible design curves for cold-formed sections loaded by compression and any level of in-plane bending is shown: the pure compression case ($\psi_2 = \psi_1 = +1$) and the pure in-plane bending case ($\psi_2 = -1$; $\psi_1 = +1$) are displayed with different colours, and the area between the lines corresponds to the various N+M_y combinations.

Once the calibration for the mono-axial cases was achieved, the formulation was expanded to account for different stress ratios in the "most compressed" plate as well, i.e. for cases with bi-axial bending, with the results given in Equ. (19) and (20). The additional multiplier as a linear function of ψ_1 covers the biaxial load case and is expressed as a variation of the formulation found in *Eurocode 3 Part 1-5* (2006) for linear stress fields in an individual plate:

$$A = 0.225 + 0.025\psi_2 \frac{(1+\psi_1)}{2} \quad \text{(cold-formed sections)} \tag{19}$$

$$A = 0.20 + 0.02\psi_2 \frac{(1+\psi_1)}{2} \quad \text{(hot-finished sections)} \tag{20}$$

The point where the slender range ends is denoted as the "elastic limit slenderness" $\bar{\lambda}_0$ and is calculated as follows: $\bar{\lambda}_0 = 0.5 + \sqrt{0.25 - A}$.

5.2 Bilinear resistance function in the plastic (stocky) range

For the plastic stocky range, two different formulations were developed in HOLLOSSTAB: a simplified bilinear function formulation and a method based on the Continuous Strength Method (CSM). The former is based on a simple expansion of the previously used, stress-based design to the stocky range, while the latter is a strain-based approach. In this paper, only this approach is described in more detail. For more details on the alternative, CSM-based approach and generally on the development of design rules in both the elastic and plastic range, see *Taras et al.* (2019). In the simplified, stress-based method, a bilinear relation was chosen to represent the resistance in the stocky range, where the cross-sectional capacity exceeds R_{el}. Two "anchor" points are needed for this purpose:

$$\chi_L = 1 \quad \text{at} \quad \bar{\lambda}_L = \bar{\lambda}_0$$

$$\chi_L = \alpha_{pl} \quad \text{at} \quad \bar{\lambda}_L = \bar{\lambda}_{pl} = 0.3$$

The proposed formulation for the prediction of the cross-section capacity for the stocky range is as follows, with the values for $\bar{\lambda}_{pl}$ and the maximum value α_{pl} (see Equ. 21) taken to represent the data with acceptable safety and accuracy. Thus, in summary, in the stocky range the GSRM design proposal reads as follows:

$$\text{For } \bar{\lambda}_L \leq \bar{\lambda}_0 : \chi_L = 1 + (\alpha_{pl} - 1)\left(\frac{\bar{\lambda}_0 - \bar{\lambda}_L}{\bar{\lambda}_0 - \bar{\lambda}_{pl}}\right) \leq \alpha_{pl} \tag{21}$$

$$\text{where } \bar{\lambda}_{pl} = 0.3; \quad \alpha_{pl} = \frac{R_{pl}}{R_{el}} \leq 1.5 \tag{22}$$

Fig. 10 illustrates the method and the resulting location of the GSRM design values of the cross-sectional (local buckling) strength $R_{b,L,design}$ for all cross-sections and load combinations studied during the numerical the parametric study. In Fig. 11a and b, the results of the parametric study – in terms of GMNIA resistance divided by the GSRM prediction for the resistance R_{el} – are plotted over the GSRM slenderness definition. The same is also done for the predictions of the GSRM in Fig. 11c and d. The figures show that the method captures the general position of the GMNIA results in the $\bar{\lambda}_L$ / χ_L plot, particularly in the slender range. The GSRM results appear to be positioned somewhat lower than the GMNIA results throughout all slenderness ranges, indicating a degree of conservatism, although the degree of conservatism is not easily assessed in this type of representation. For this purpose, the ratios between strength predictions were determined in the next section.

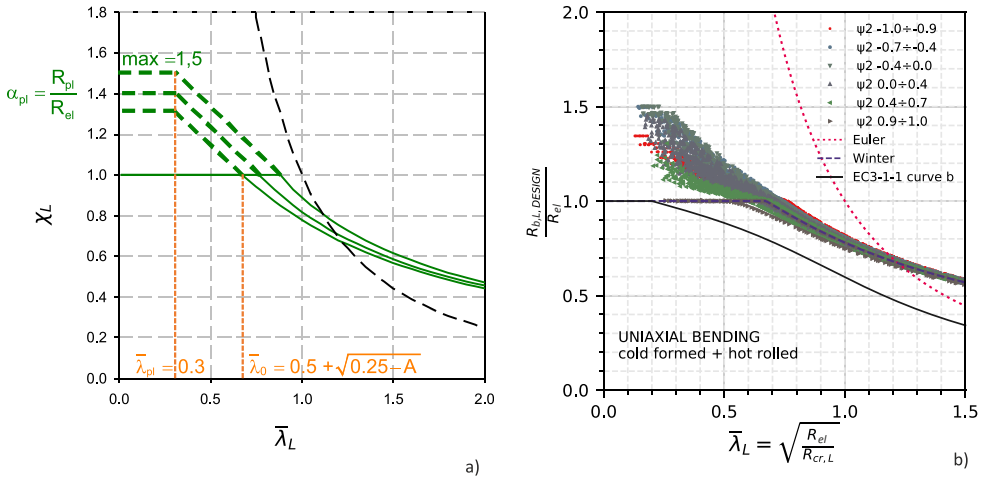

Fig. 10: a) representation of the simplified bilinear relation in the stocky range and Winter formulation in the slender range, b) evaluation of the hot-finished and cold-formed sections dataset for the uniaxial bending case (ψ_1=1, ψ_2 varies from -1 to 1).

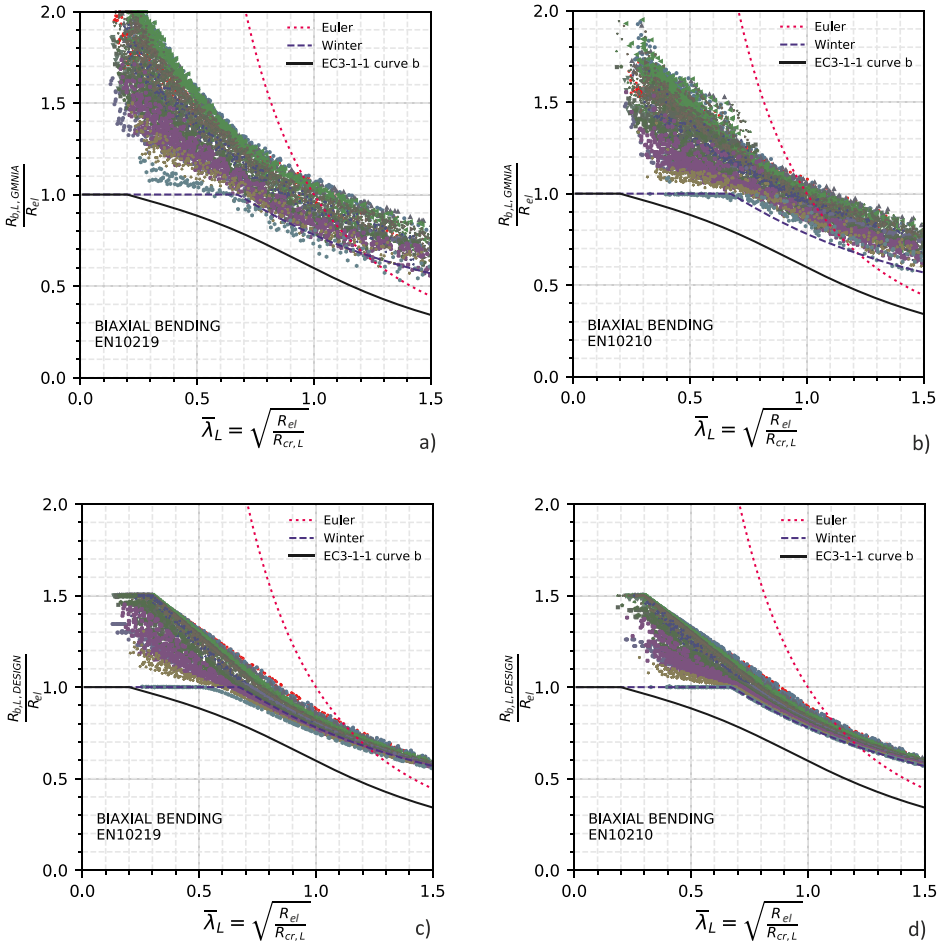

Fig. 11: Representation of the GMNIA results for a) cold-formed sections and b) hot-finished sections in the case of biaxial bending, where the different colours represents different ranges and combinations of ψ_1 and ψ_2; in c) and d) the corresponding values according to the GRSM proposal are represented

6 Comparison of FEM results vs. GSRM and code rules

In this section, the results of the numerical parametric study are compared to the new GSRM design rules for the cross-sectional capacity of SHS and RHS, as well as to the current design rules found in the prEN-version of Eurocode 3 and the AISC design specifications. Fig. 12a gives an overview of accuracy and safety of the new GSRM design rules by normalizing the numerical test results by the rule in the GRSM, see sub-plot a). In addition, the results of the GMNIA and the design method (sub-plot b) are also compared with the EC3 design results in the latest prEN-version of *EN 1993 part 1-1* (2018), including the method found in the new Annex B of this standard and developed in the RFCS-project SEMI-COMP (*Greiner et al. 2008*) for the EC3-based design of "semi-compact" (class 3) cross-sections. Fig. 12c compares the tests with the AISC rules (*ANSI/AISC 360-16 2016*). The indices "GMNIA", "GSRM", "AISC" and "EC3" thus refer to GMNIA numerical results, the new GSRM design proposal, the AISC and prEN 1993 part 1-1 (*2018*) design rules, including this standard's Annex B.

Fig. 12a shows that the GSRM design displays a very consistent level of accuracy and comparable average distance from the GMNIA resistances across all slenderness ranges. The EC3 design rules, on the other hand, show much larger inconsistencies and larger scatter in the results for classes 1 to 4, see Fig. 12b. The AISC rules produce uniform and large scatter over different levels of slenderness and a generally decreasing safety level with increasing slenderness (sub-plot c). Thereby, the AISC design rules considerably simplify the design procedure compared to the EC3 rules, with an important side-effect though being a clear lack of precision, especially in the slender range. It should however be noted that, in the figure, all resistance predictions were obtained without applying safety factors, in order to compare characteristic resistances in all cases.

Gains in strength through the use of the GSRM compared to the current EC3 design strengths are thus noticeable particularly for class 4 sections. A - consciously accepted - lower resistance is found for class 1 and 2 sections, in order to compensate for an apparent lack of conservatism of the Eurocode rules in this range when compared to numerical tests. For class 3 sections, the methods are on average equivalent in their strength predictions. For high-strength steel sections, which almost exclusively fell in class 3 or (more often) 4, the gains in strength were on average above 10%, and above 15% for class 4 sections. In cases with a pronounced level of bending biaxiality, the gains are even higher.

When directly compared to the AISC rules, the GSRM predicts on average a very comparable strength in the stockier EC3 classes 1, 2 and 3 (1-3% higher, see Fig. 12d) and 11% lower strength predictions for the class 4 section, again disregarding the impact of safety factors. It shall however be noted that the safety factor proposed for the GSRM method is 1.0, while the AISC rules would require a lowering of all values by a LRFD resistance factor of at most 0.9, thus bringing down the average design resistances to the level of the GSRM prediction even in the stocky range.

In all cases, particularly those that involve load cases with combined compression and bending, the GSRM design method employs a much more straightforward design methodology than the Eurocode and avoids the cumbersome determination and use of effective cross-sections (class 4 sections) respectively of multi-step design strengths for combined loading (class 1 to 3). The statistics of these data, which are also represented in Fig. 12, are summarized in
Table 2.

Table 2: Summary of the results average value (m) and standard deviation (s)

		Class 1 and 2	Class 3	Class 4
$\frac{R_{b,L,GMNIA}}{R_{b,L,GSRM}}$	m	1.12	1.11	1.12
	s	0.09	0.05	0.05
$\frac{R_{b,L,GMNIA}}{R_{b,L,EC3}}$	m	1.04	1.10	1.25
	s	0.09	0.07	0.13
$\frac{R_{b,L,GMNIA}}{R_{b,L,AISC}}$	m	1.16	1.12	0.99
	s	0.17	0.15	0.13
$\frac{R_{b,L,GSRM}}{R_{b,L,AISC}}$	m	1.03	1.01	0.89
	s	0.12	0.12	0.11

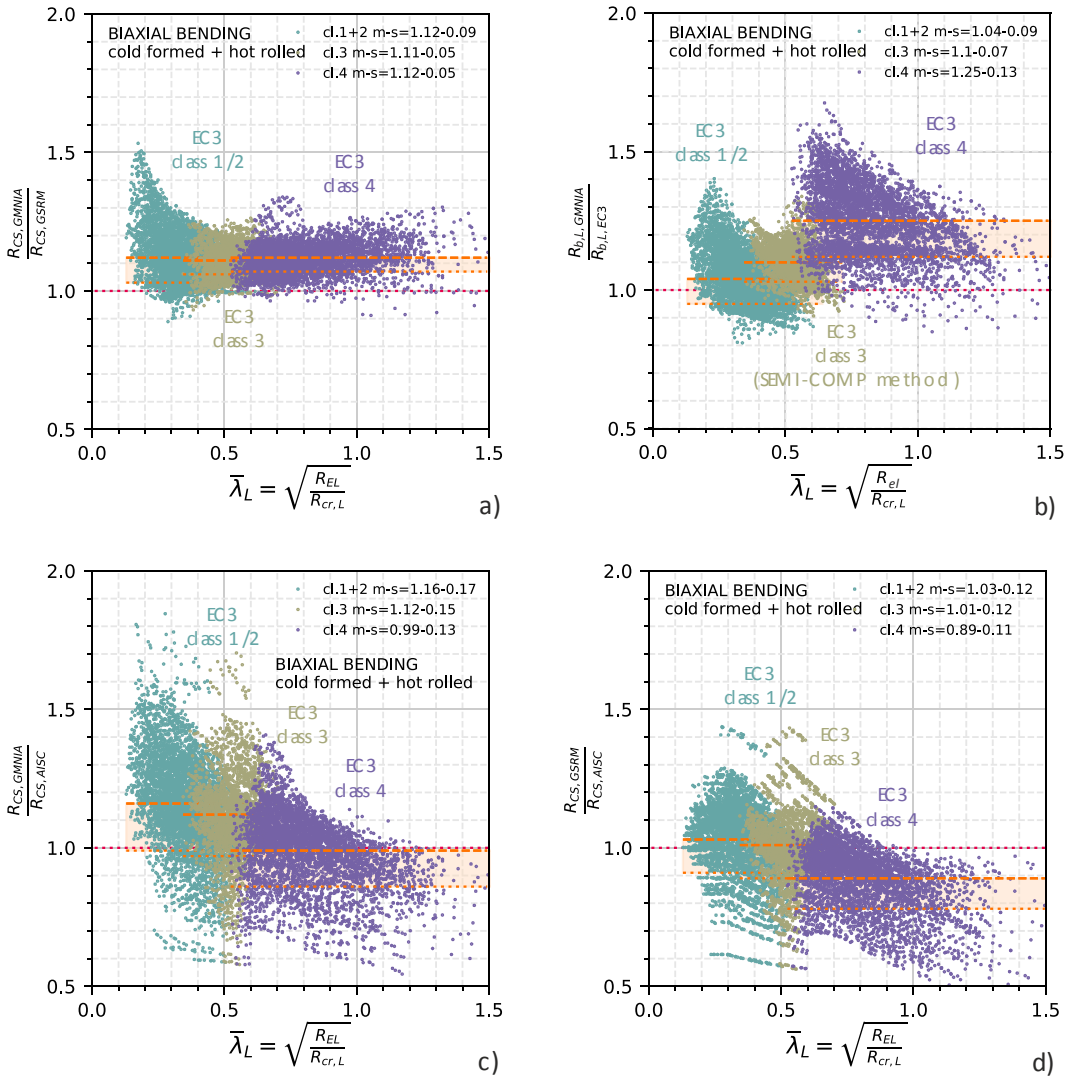

Fig. 12: Validation of the GSRM rules vs. GMNIA, AISC and EC3 design rules: a) GMNIA results normalized by the GSRM results, plotted over slenderness; b) GMNIA vs. EC3 results; c) GMNIA vs. AISC; d) GSRM vs. AISC.

7 Summary and Conclusions

This paper describes and provides the background to a new design method for the determination of the cross-sectional capacities of SHS and RHS made of mild or high-strength steel and loaded by any combination of axial (compressive) forces and bending moments about one or both principal axes of rotation. The new method, termed the Generalized Slenderness-based Resistance Method (GSRM), makes use of a generalization of the slenderness definition, which is commonly determined with the aid of dedicated numerical tools. The generalized slenderness is the main input parameter for the calculation of strength, given as a (direct) function of this slenderness. The GSRM developed during HOLLOSSTAB may be applied to various types and shapes of hollow sections and for cross-sections as well as members. As stated, this paper has restricted itself to the GSRM design for the cross-sectional capacities of SHS and RHS as well as to only one of two alternative approaches in the non-elastic range. The results of the GSR method are compared with well-known American and the European code predictions for the cross-section resistance, demonstrating significant improvements in consistency, safety and cross-section strength. In addition, HOLLOSSTAB also led to the development of a second, strain-based (CSM) approach for the design of stockier cross-sections as well as the GSRM design rules for the global buckling of members. Further details of the design of members can be found in *Taras et al.* (2019b) and will shortly be published in additional journal papers.

Acknowledgments

The authors would like to acknowledge the funding received by the European Community's Research Fund for Coal and Steel (RFCS) under grant agreement No. 709892 - HOLLOSSTAB. In addition, they would like to acknowledge the kind external support of the project, through the supply of test specimens and workshop hours, of voestalpine Krems Finaltechnik GmbH, Krems (Austria) and Vallourec Germany GmbH, Düsseldorf (Germany).

References

Afshan, S., Gardner, L. (2013): The continuous strength method for structural stainless steel design, *Thin-Walled Structures*, 68, pp. 42–49, London/Amsterdam: Elsevier.

AISI S100-16 (2016), North American Specification for the Design of Cold-Formed Steel Structural Members, *American Iron and Steel Institute*

ANSI/AISC 360-16 (2016), Specification for Structural Steel Buildings, American Institute of Steel Construction, Chicago IL.

Boissonnade, N.; Hayeck, M.; Saloumy, E.; Nseir, J. (2017): An Overall Interaction Concept for an alternative approach to steel members design, *Journal of Constructional Steel Research*, 135, pp.199-212, London/Amsterdam: Elsevier.

EN 10219 (2006): Cold formed welded structural hollow sections of non-alloy and fine grain steels, *CEN – European Committee for Standardization*, Brussels.

EN 10210 (2006): Hot finished structural hollow sections of non-alloy and fine grain steels, *CEN – European Committee for Standardization*, Brussels.

Eurocode 3 (2006): Design of steel structures - Part 1-5: General rules - Plated structural elements, *CEN - European Committee for Standardization*, Brussels, version EN 1993-1-5.

Eurocode 3: (2018) Design of steel structures – Part 1-1: General rules and rules for buildings, *CEN - European Committee for Standardization*, Brussels, Draft standard under review by National Standardisation Bodies, version prEN 1993-1-1.

Fieber, A., Gardner, L., Macorini, L. (2019): Design of structural steel members through advanced inelastic analysis with strain limits, *Engineering Structures*.

Gardner, L. (2008): The Continuous Strength Method, *Structures & Buildings* 161(3), pp.127-133, Elsevier, London.

Gardner, L., Yun, X. (2018): Description of stress-strain curves for cold-formed steels, *Construction and Building Materials*, 189, pp. 527–538, London/Amsterdam: Elsevier.

Gardner, L., Yun, X. (2017): Strain-stress curves for hot-rolled steels, *Journal for Constructional Steel Research*, 133, pp. 36-46, London/Amsterdam: Elsevier.

Greiner, R.; Kettler, M.; Lechner, A.; Freytag, B.; Linder, J.; Jaspart, J.-P.; Boissonnade, N.; Bortolotti, E.; Weynand, K.; Ziller, C.; Oerder, R. (2008): Final Report: SEMI-COMP: Plastic Member Capacity of Semi-Compact Steel Sections - a more Economic Design, Research Fund for Coal and Steel *Project SEMI-COMP, Grant Nr. RFSR-CT-2004-00044*.

Kettler, M., Greiner, R. (2009): Ein „Overall-Konzept“ für die Querschnittstragfähigkeit im elasto-plastischen Bereich, Stahlbau, 78 (10), pp. 742-749, Berlin: Wiley / Ernst&Sohn

Meng, X., Toffolon, A., Gardner, L., Taras, A. (2019): Generalised slenderness-based resistance method for design of CHS and EHS, *Steel Construction*.

Rusch, A.; Lindner, J. (2001): Überprüfung der grenz (b/t)-Werte für das Verfahren Elastisch-Plastisch, *Stahlbau*, 70, pp. 857-868, Berlin: Wiley / Ernst&Sohn.

Schafer, B.W. (2008): Review: The Direct Strength Method of cold-formed steel member design, *Journal of Constructional Steel Research*, 64, Issue 7-8, pp. 766-778, London/Amsterdam: Elsevier.

Schafer, B. W. (2018): Advances in the direct strength method of thin-walled steel design, *Eighth International Conference on Thin-Walled Structures (ICTWS)*.

Schillo, N.; Taras, A.; Feldmann, M. (2018): Assessing the reliability of local buckling of plates for mild and high strength steels, *Journal of Constructional Steel Research*, 142, pp. 86-98, London/Amsterdam: Elsevier.

Szalai, J.; Papp F. (2011): Theory and Application of the General Method of Eurocode 3 Part 1-1, *Proc. of EUROSTEEL 2011*, Budapest, Hungary.

Tankova, T.; Marques, L.; Andrade, A.; Simões da Silva, L. (2017): A consistent methodology for the out-of-plane buckling resistance of prismatic steel beam-columns, *Journal of Constructional Steel Research*, 128, pp. 839-853, London/Amsterdam: Elsevier.

Taras, A. (2016): Derivation of DSM-type resistance functions for in-plane global buckling of steel beam-columns, *Journal of Constructional Steel Research*, 105, pp. 95-113, London/Amsterdam: Elsevier.

Taras, A.; Toffolon, A.; Niko, I.; Gardner, L., Meng, X., Silvestre, N. (2019a): Cross-sectional resistance / local buckling of RHS & SHS, HOLLOSSTAB, *RFCS Grant Nr. 2015-709892*, Deliverable 4.2, Munich.

Taras, A.; Toffolon, A.; Gardner, L.; Meng, X. (2019b): Background on the development of Overall-Slenderness based design rules for RHS and SHS, HOLLOSSTAB, RFCS Grant Nr. 2015-709892, Deliverable 8.2, Munich.

Toffolon, A.; Taras, A. (2019a): Development of an OIC-Type local buckling design approach for cold-formed unstiffened and groove-stiffened hollow sections, *Thin-Walled Structures*, 144.

Toffolon, A.; Müller, A.; Niko, I.; Taras, A. (2019b): Experimental and numerical analysis of the local and interactive buckling behaviour of hollow sections, *Proceedings of SDSS 2019*, Prague.

Winter, G. (1946): Strength of thin steel plates compression flanges, *Transactions of the American Society of Mechanical Engineers*, 112(1), pp. 527-554

Yun, X., Gardner, L., Boissonnade, N. (2018a): The continuous strength method for the design of hot-rolled steel cross-sections, Engineering Structures, 157, pp. 179-191, London/Amsterdam: Elsevier.

Yun, X.; Gardner, L. (2018b): The continuous strength method for the design of cold-formed steel non-slender tubular cross-sections, Engineering Structures, 175, pp.549-564, London/Amsterdam: Elsevier.